Journal of Molecular Structure 1225 (2021) 129299

Contents lists available at ScienceDirect

Journal of Molecular Structure

journal homepage: www.elsevier.com/locate/molstr

Experimental investigation of structural, surface, optical and electrical properties of gallium sesquioxide doped tausonite compounds

G. Saravanan [a], K. Ramachandran [a,*], J. Gajendiran [b], S. Gnanam [c]

[a] Department of Physics, SRM Institute of Science and Technology, Vadapalani Campus, Chennai 600 026, India
[b] Department of Physics, Vel Tech Rangarajan Dr.Sagunthala R&D Institute of Science and Technology, Avadi, Chennai 600 062, India
[c] Department of Physics, School of Basic Sciences, Vels Institute of Science, Technology & Advanced Studies (VISTAS), Pallavaram, Chennai 600 117, Tamilnadu, India

ARTICLE INFO

Article history:
Received 24 July 2020
Revised 11 September 2020
Accepted 17 September 2020
Available online 18 September 2020

Keywords:
$SrTiO_3$
Structural properties
Optical properties
Dielectric properties
Electrical properties

ABSTRACT

We report that 1% and 3% wt concentration of gallium sesquioxide (Ga_2O_3) doped tausonite ($SrTiO_3$) compounds have been developed by mechanochemical synthesis followed by calcination process and their microstructural, spectral and opto-electrical characterization are discussed for the first time. The lattice parameter values of the Ga_2O_3 doped $SrTiO_3$ samples were examined using the X- ray Diffraction (XRD) and Williamson-Hall (W-H) plot. The cubic structure of $SrTiO_3$ is confirmed by the XRD and Raman studies. The Field Effect-Scanning Electron Microscopy (FE-SEM) images of the Ga_2O_3 doped $SrTiO_3$ samples were composed of spherical particles with agglomeration throughout the surface. The chemical elements and chemical states of the prepared compound have been tested in the Fourier Transform Infrared (FT-IR), Energy Dispersive X-ray (EDX) and X-ray Photoelectron Spectroscopy (XPS) studies. The optical spectra displayed that the absorption wavelength shifted near the red shift with the increase of the Ga_2O_3 doped $SrTiO_3$. The dielectric and electrical conductivity responses of the 1% and 3 wt % Ga_2O_3 doped $SrTiO_3$ materials were investigated in the dielectric and electrical studies.

1. Introduction

The incorporation of transition metals or non-metals or mixed transition ions doping in tausonite ($SrTiO_3$) material and its consequences can alter the size, shape, optical absorption, and optical band gap of the particles and the photocatalytic, magnetic, thermal and electrical properties. This is due to the dopants creating the distortion of the lattice or surface modification in tausonite. $SrTiO_3$ has some unique properties, such as the formation of paraelectric or ferroelectric material depending on room temperature or low temperature, good structural and thermal stability, broad optical band gap and optical absorption in the ultraviolet portion and large dielectric constant [1–31]. These unique properties which satisfy the material of $SrTiO_3$ material and may be suitable for a wide range of applications like optical and electronic devices, photocatalysts, gas sensors, spintronics, and high frequency tunable devices [1–31].

Over the last few years, the doping effects of transition metals (Fe, Cr, Mn, Sn, Co) [1–11], non-metals (N, C) [12,13], rare earth metals (La, Nd, Y, Nb, Gd, Er, Pr, Sm, Ce) [17–27] and mixed two elements (La/Fe, La/Co, La/Dy, La/Y, Bi/Cu, Cu/Nb, Bi/Li) [24–31] have been applied to $SrTiO_3$ materials by different chemical methods, such as solid state reaction, ball milling, sol-gel, combustion, solvothermal, hydrothermal etc. The literatures referred to above investigated the impact of dopants on the crystal structure, particle size and shape, lattice parameters, optical, catalytic and electrical responses of $SrTiO_3$ for optoelectronic devices, photocatalysts etc. Based on the above literatures, the preparation of the doped $SrTiO_3$ material requires certain conditions like autoclave, high pressure, above 1000 °C temperature, microwave, vacuum, ultrasonicator and inert gas (He or N_2 or H_2/N_2) and sometimes a secondary phase etc. In this work, we used Ga_2O_3 as a doping material for $SrTiO_3$ material. Ga_2O_3 material has multifunctional properties like wide optical band gap and good insulator for dielectric coating and optoelectronic device applications. We have prepared Ga_2O_3 doped $SrTiO_3$ materials using a solid state synthesis method, sintering at 1000 °C without using any solvent, autoclave, vacuum, inert gas etc. The novelty of this present work is that the effects of Ga_2O_3 doping on crystal structure and strain, crystallite and particle size and shape, energy gap and electrical activity (relative permittivity, dielectric loss and electrical conductivity) of the tausonite compounds have been studied and reported for the time.

* Corresponding author.
E-mail address: kaviramach76@gmail.com (K. Ramachandran).

https://doi.org/10.1016/j.molstruc.2020.129299
0022-2860/

2. Experimental

2.1. Materials

Strontium ($SrCO_3$) (Merck), titanium dioxide (TiO_2) (Merck) and gallium sesquioxide (Ga_2O_3) (Merck) were obtained commercially and used as received without further purification.

2.2. Preparation of Ga_2O_3-doped $SrTiO_3$ powders

Ga_2O_3-doped tausonite materials were produced by mixing carbonate salt of strontium ($SrCO_3$), titanium dioxide (TiO_2) and gallium sesquioxide (Ga_2O_3) as a dopant via the mechanochemical synthesis followed by a calcination process. 3.20 g of $SrCO_3$, 1.68 g of TiO_2 0.04 and 0.12 g of Ga_2O_3 (1 and 3 wt%) selected compounds were measured and the following chemicals were admixed together to be in a hot plate pre heated at 200 °C for 1hr. Further, the obtained mixed chemicals' powder was well ground for 1 hr in an agate mortar, followed by calcination at 400 °C for 6 hrs in a muffle oven. The reason for the choosing the above calcined temperature was to completely eliminate the carbonate from the mixed powder. Furthermore, the above burnt powder was transferred to the mortar and well ground for 3600 seconds. After that, the fine ground powder was kept in an alumina crucible and preserved in the furnace sintered at 1000 ° C for 6 hrs. After ample cooling, the Ga_2O_3 doped tausonite ($SrTiO_3$) powders were taken out from the electronic furnace.

The probable formation mechanism of the Ga_2O_3 doped $SrTiO_3$ compounds are expressed below: [24].

$$Sr_{(1-x)}CO_3 + TiO_2 + x(Ga_2O_3) \rightarrow Sr_{(1-x)}TiO_3 : x(Ga) + CO_{2\uparrow} \quad (1)$$

Where x = 1% and 3% gallium sesquioxide dopant concentration.

2.3. Characterization

The crystal phase of the prepared ceramic compounds was characterized with the assistance of the X'pert PRO XRD instrument (Cuk_α=1.54056Å). The chemical bond between the elements was examined by the Nicolet spectrometer- model 6700 FTIR spectra. The crystal phase was identified by the Renishaw in the VIA model Raman spectrometer instrument using the laser light as an excitation source with an optical wavelength of 785 nm. The surface morphology and chemical elemental analysis were examined by the HITACHI S-3400N. The optical behavior was tested on the Shimadzu- UV-VIS-NIR spectrometer instrument. Chemical states were detected through the PHI 5000 versa probe III-XPS instrument. The calcined ceramic compounds were pelletized; polished and a single electrical conductor made of copper was fixed using silver paste coated on two faces of the pellet, which reacts as a conductive (electrode) material. Then, the dielectric properties were studied on the HIOKI 3532-50 LCR Hi TESTER instrument for different temperatures (305 K to 573 K) and recorded at different frequencies ranging between 10^2 and 10^6 Hertz.

3. Results and discussions

3.1. Powder X-ray diffraction (XRD) analysis

We have already reported the preparation of pure $SrTiO_3$ material via the solid state reaction method and its powder XRD pattern [23]. In this present work, we have prepared 1% and 3 wt% concentrations of gallium sesquioxide doped $SrTiO_3$ and their XRD pattern is displayed in Fig. 1 (a&b). The powder XRD patterns of the doped samples were recorded at the diffraction angle (2θ) in the range of 20 ° to 80 ° on the x-axis and the intensity on the y-axis for the determination of their crystalline phase.

The XRD patterns of the Ga_2O_3-doped $SrTiO_3$ samples indicated the reflected diffraction peaks of (100), (110), (111), (200), (210), (211), (220) and (310) planes, respectively. The detected sharp reflected diffraction planes and peak positions were compared to the reported reflected peak positions of the $SrTiO_3$ compound in the XRD pattern. After examining the obtained reflected peak position in the XRD pattern with the reported reflected peak position, the prepared 1% and 3% Ga_2O_3 doped $SrTiO_3$ samples confirmed the formation of cubic perovskite crystal structure of the $SrTiO_3$ compound (JCPDS.No.01-084-0443) [23]. However, there was no modification in the crystalline phase of the XRD pattern of the synthesized samples by the addition of the Ga_2O_3 doping to the host lattice. This was due to the difference between the ionic radii of the dopant (Ga = 00.62 nm) and the parent ions (Sr = 0.132 nm) [35] which confirmed the incorporation of Ga_2O_3 into the strontium titanate lattice. Further, no additional impurity compounds, such as Ga_2O_3 or $SrCO_3$ were found in the XRD pattern of the synthesized gallium doped $SrTiO_3$ samples, suggesting the confirmed formation of a mono phase with high phase purity. The purpose of adding a lower concentration of Ga_2O_3 doping was to retain the high purity single phase of the prepared $SrTiO_3$ material. Suppose, we increase the dopant concentration in the host material, it can create a secondary phase in the XRD pattern. In addition, the sharp diffraction peaks showed that the prepared Ga_2O_3-doped $SrTiO_3$ samples were of a very crystalline nature. The XRD pattern of the 3% Ga_2O_3-doped $SrTiO_3$ sample indicated that the high intensity reflection plane (110) was shifted to a higher angle with a slightly narrow broadening peak compared to that of the 1% Ga_2O_3-doped sample, as shown in Fig. 1b, which may increase the crystallite size due to the lattice deformation (strain). In addition, we observed increasing cystallinity with the increasing of the Ga_2O_3 dopant concentration in the $SrTiO_3$ material. The mean size of crystallites (D) was calculated from the XRD pattern through Scherer's equation [24]:

$$D = k\lambda/\beta\cos\theta \quad (2)$$

Where, λ is the wavelength of the Cuk_α radiation (0.15405 nm), θ is the diffraction angle and k is a geometric factor (k = 0.89 for spherical particles). Full Width Half Maximum (FWHM) values are detected from the high intensity peak of (110) in the XRD pattern of the Ga_2O_3 doped samples.

The FWHM values are detected to be 0.2521 and 0.2389 from the sharp intensity peaks (110) at diffraction angles located at 32.44° and 32.64°, respectively for the 1% and 3% Ga_2O_3 doped $SrTiO_3$ samples. After that the above FWHM and reflected angle position values are substituted in Scherer's equation and it was determined that the crystallite sizes were 36.5 and 38.5 nm respectively, for 1% and 3% Ga_2O_3-doped $SrTiO_3$ samples. Based on the above findings, the crystalline size of the $SrTiO_3$ compound increased with an increase in the concentration of Ga_2O_3 dopant in the XRD pattern. Some lattice parameter values of the Ga_2O_3 doped samples have been computed from XRD data and are given in Table 1.

From Table 1, we could notice decreasing d-spacing, lattice constant and volume of the unit cell with increasing the Ga_2O_3 doped concentration in the $SrTiO_3$ sample. The calculated lattice parameter values of the Ga_2O_3 doped $SrTiO_3$ samples, are comparable with the previously reported lattice parameter values of the doped $SrTiO_3$ material [1,3,5,31].

3.2. Williamson-Hall (W-H) plot analysis

The average crystallite size (D) and crystalline strain (ε) values of 1% and 3% Ga_2O_3 doped STO was determined through the Williamson-Hall (W-H) plot by using this formula: [24]

$$\beta\cos\theta = k\lambda//D + \varepsilon(4\sin\theta) \quad (3)$$

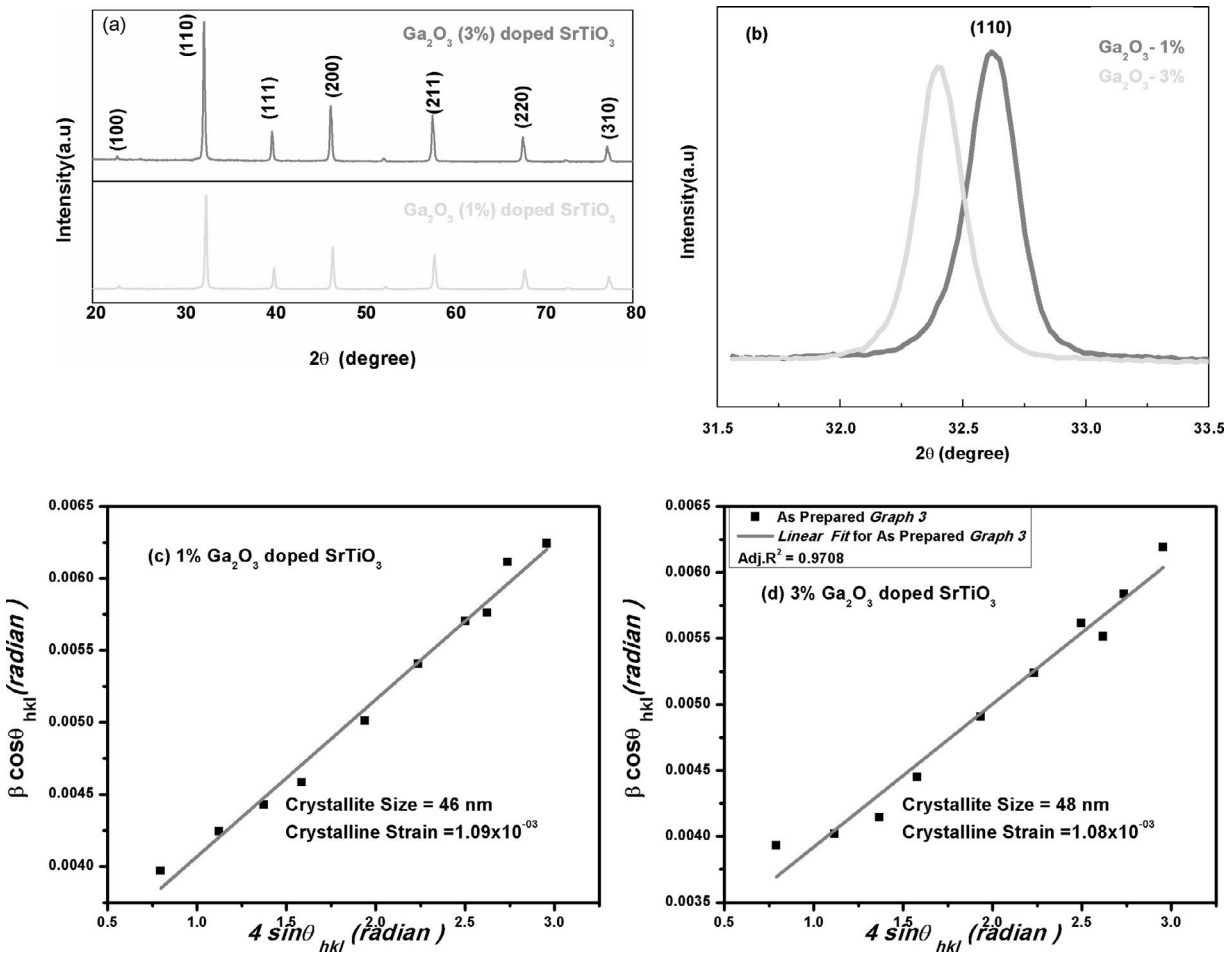

Fig. 1. (a) XRD pattern of Ga_2O_3 (1% & 3%) doped $SrTiO_3$ samples. (b) High Intensity diffraction peak (110) of Ga_2O_3 (1% & 3%) doped $SrTiO_3$ samples. W-H plot of (c) 1% and (d) 3% Ga_2O_3-doped $SrTiO_3$ samples.

Table 1
Some lattice parameter values of the Ga_2O_3 doped samples were computed from the XRD data.

Ga_2O_3 doped $SrTiO_3$ samples	d-spacing values are calculated by using formula $d = n\lambda/2\sin\theta$ (Å)	Lattice constant (a) values are calculated by using formula $a = d/\sqrt{(h^2+k^2+l^2)}$ (Å)	Volume of the unit cell $(a)^3$ $(Å)^3$
1% Ga_2O_3 doped $SrTiO_3$	2.73	3.86	57.51
3% Ga_2O_3 doped $SrTiO_3$	2.70	3.82	55.74

Table 2
Crystallite size and strain, slope, intercept, Adj R^2 of the Ga_2O_3 doped $SrTiO_3$ samples using W-H plot with the assistance of linear fit curves.

Ga_2O_3 doped $SrTiO_3$ samples	Crystallite size estimated by using W-H plot	Crystalline strain	Intercept	Slope	AdjR^2 using linear fit
1% Ga_2O_3	46 nm	1.09×10^{-3}	0.0029	0.0010	0.9866
3% Ga_2O_3	48 nm	1.08×10^{-3}	0.00284	0.00108	0.9708

The average crystallite size and crystalline strain values of the1% and 3% Ga_2O_3 doped $SrTiO_3$ were determined through the Williamson-Hall (W-H) plot using the XRD data and their determined values are mentioned in plots (Fig. 1.c). The crystallite size and strain, slope, intercept, and Adj R^2 of the Ga_2O_3-doped $SrTiO_3$ samples using the W-H plots with the assistance of linear fit curves are given in Table 2. From Table 2 we could observe the increasing crystallite size and intercept, and decreasing slope and AdjR^2 values on increasing the Ga_2O_3 concentration in the $SrTiO_3$.

We noticed the increasing average crystallite size and decreasing crystalline strain with the increase in the dopant concentration in the $SrTiO_3$ (Table 2). The estimated average crystallite size values are comparable with the calculated crystallite size using Scherer's formula. The crystalline strain is directly related to the crystal imperfections like dislocation or oxygen vacancy [32]. In ad-

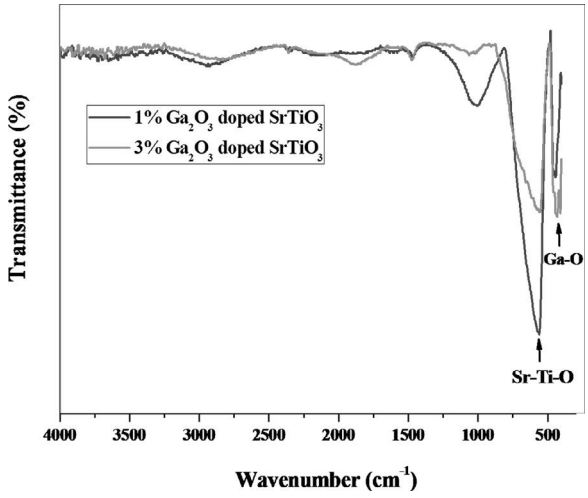

Fig. 2. FT-IR spectra of Ga_2O_3 (1% & 3%) doped $SrTiO_3$ samples.

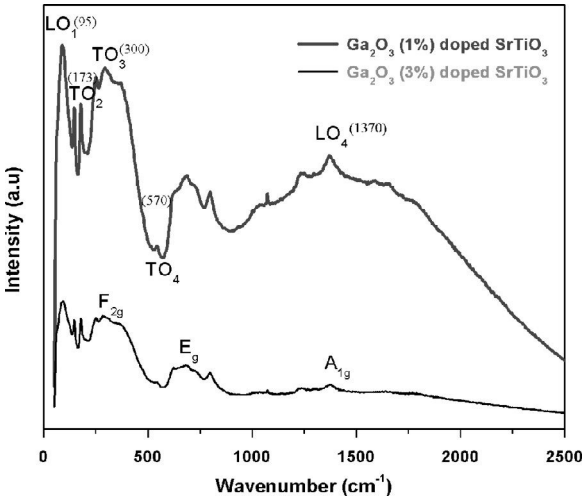

Fig. 3. Raman spectra of Ga_2O_3 (1% & 3%) doped $SrTiO_3$ samples.

dition, the dislocation density is inversely proportional to the volume of the unit cell. Thus, from Table 1, we found that the dislocation density is slightly higher for the 3% Ga_2O_3 doped $SrTiO_3$ compared to that of the 1% Ga_2O_3 doped sample using the volume of the unit cell, which indicates that a slightly higher value of strain for the 3% Ga_2O_3 doped sample is indirectly correlated with the obtained strain values of the Ga_2O_3 doped samples, as seen from the W-H plot. Dislocation plays a vital role in the resistance switching phenomenon [32].

3.3. Fourier transform infrared (FT-IR) spectra analysis

We plotted the wavenumber on the x-axis vs transmittance on the y-axis to identify the interaction between the chemical elements of the synthesized Ga_2O_3-doped strontium titanate, as represented in Fig. 2. We recorded a wavenumber range of 4000-400 cm^{-1} for the detecting chemical bonds. The intense absorption bands appeared in the wavenumber range of 400-700 cm^{-1}, and are assigned to the normal characteristic stretching modes of the metal oxides (M-O) of stronium-oxygen (Sr-O), titanium-oxygen (Ti-O), gallium-oxygen (Ga-O) and titanium-oxygen-titanium (Ti-O-Ti) [33]. These types of normal characteristic modes were reported in the electromagnetic radiation of infrared (IR) bands wavenumbers less than 1000 cm^{-1}. This was due to the deformation modes of titanium-oxygen (Ti-O) bonds in the TiO_6 octahedran stretching mode distortion or the distortion of Ti-O-Ti bridges. There was no additional band perceived in the FT-IR spectra, which indicated that the prepared samples corroborate the formation of strontium titanate material.

3.4. Raman spectra analysis

The vibrational-rotational spectra are generally plotted between the wavenumber on the x-axis and intensity on the y-axis to detect the chemical bond elements. This plot is commonly called the Raman spectroscopic study. The Raman spectra of the Ga_2O_3 doped $SrTiO_3$ samples are laid out in Fig. 3. In both the Ga_2O_3 doped $SrTiO_3$ samples, two broad scattering peaks appear around as (230-410) and (610-760) cm^{-1} in the Raman spectra, which represent the second order Raman scattering modes respectively. In general, $SrTiO_3$ exhibits a cubic structure, so that Raman scattering was allowed only for second order. This was due to the presence of a broad active lattice vibration (phonon) mode [34].

The first order Raman scattering was not allowed because the lattice vibration mode becomes null at the middle of the allowed energy region (Brillouin zone). The Raman spectra of the active intense peak was noticed around 110 and 610 cm^{-1} and ascribed to the longitudinal optical phonon and transverse modes [35], respectively. The transverse optical modes TO_2 and TO_4 were assigned to the bending mode vibrations of oxygen. In addition, the transverse optical mode TO_3 represents the rotation of oxygen ions [36]. The longitudinal phonon (LO_4) mode peak at 1370 cm^{-1} reveals the wider, due to the induced deformation arising from an irregular distribution of Ga_2O_3 in the $SrTiO_3$ surface lattice [37]. The peak intensity keeps on the Raman LO mode increasing for 3% Ga_2O_3 doped $SrTiO_3$ a small active phonon mode seems around as 1076 cm^{-1}. This was due to the degrees of lattice vibration was disturbed by the incorporation of Ga_2O_3 dopant in cubic structured $SrTiO_3$ material.

3.5. Field effect-scanning electron microscopy (FE-SEM) analysis

We have given the undoped $SrTiO_3$ sample micrographs for comparison with the Ga_2O_3 doped $SrTiO_3$ samples micrographs (FE-SEM) for finding the variation of the microstructural behavior (Fig. 4 (a-c)). This was due to the surface modification that occurred (ie. particulate systems likely to change their total surface tension) when increased Ga_2O_3 dopant concentration was incorporated into the host lattice of $SrTiO_3$. In addition, we could notice the distinct morphology like cubical particles, spherical particles with non-uniform size and irregular sheets/spherical particles (as inset with a blue arrow in Fig. 4) for the undoped, 1% and 3% Ga_2O_3 doped $SrTiO_3$ samples. In addition, particles are clearly visible, suggesting that the prepared Ga_2O_3 doped $SrTiO_3$ samples are quite crystalline in nature.

3.6. UV-visible absorption spectra analysis

The UV-Visible absorption spectra and Tauc plot of the Ga_2O_3 doped $SrTiO_3$ samples are depicted in Fig. 5 (a&b). In general, if a sharp optical absorption edge is found in the optical absorption spectra, the optical band gap energy could be calculated directly using the energy gap formula $E_g = 1240/\lambda_{abs}$. This energy gap is called the direct band gap.

However, the absorption peak of Ga_2O_3 doped $SrTiO_3$ samples is not detect sharp band edge; so it exhibits an indirect band gap nature of $SrTiO_3$ compound. We will find out the optical energy gap energy values from the indirect energy band gap na-

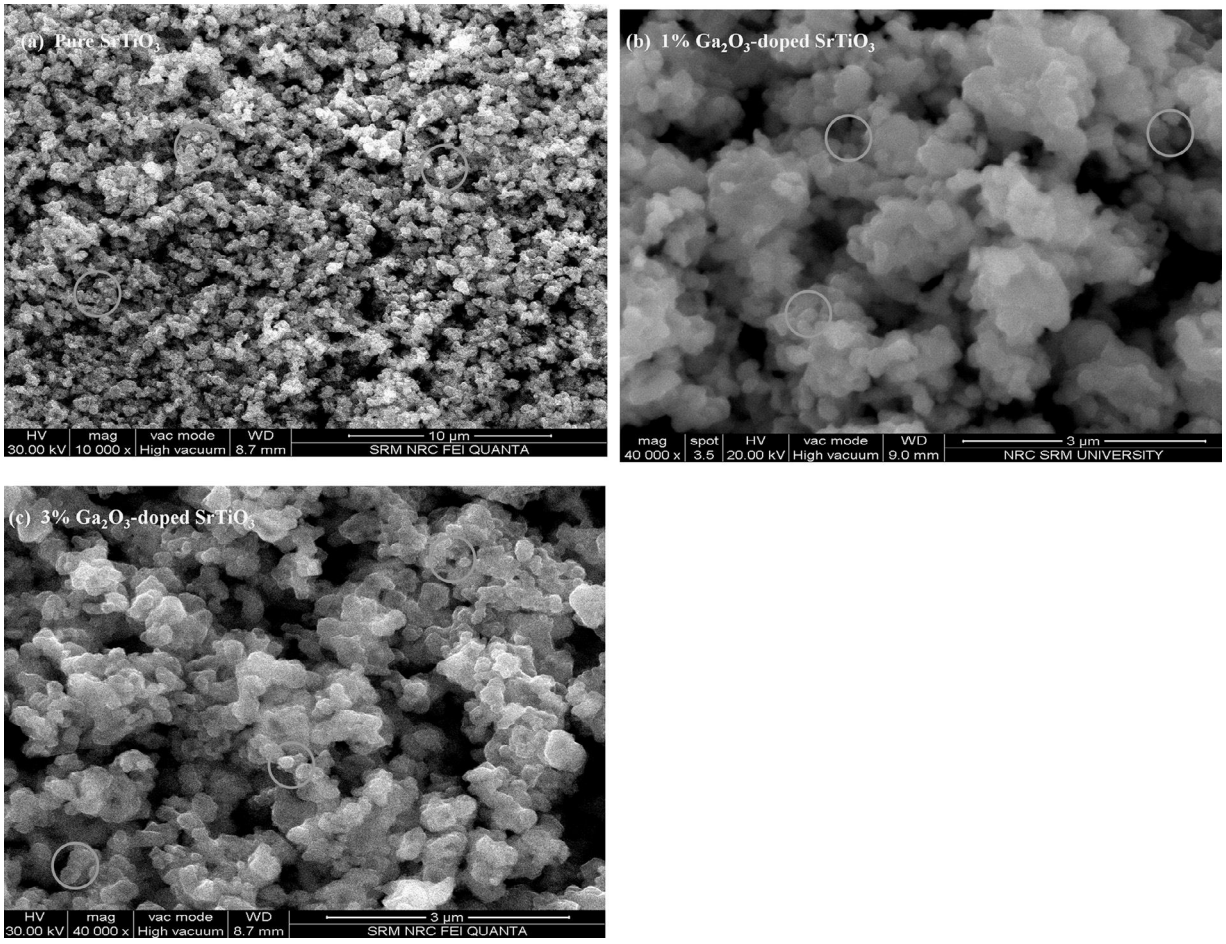

Fig. 4. FE-SEM images of (a) undoped $SrTiO_3$, (b) 1% and (c) 3% Ga_2O_3-doped $SrTiO_3$ samples.

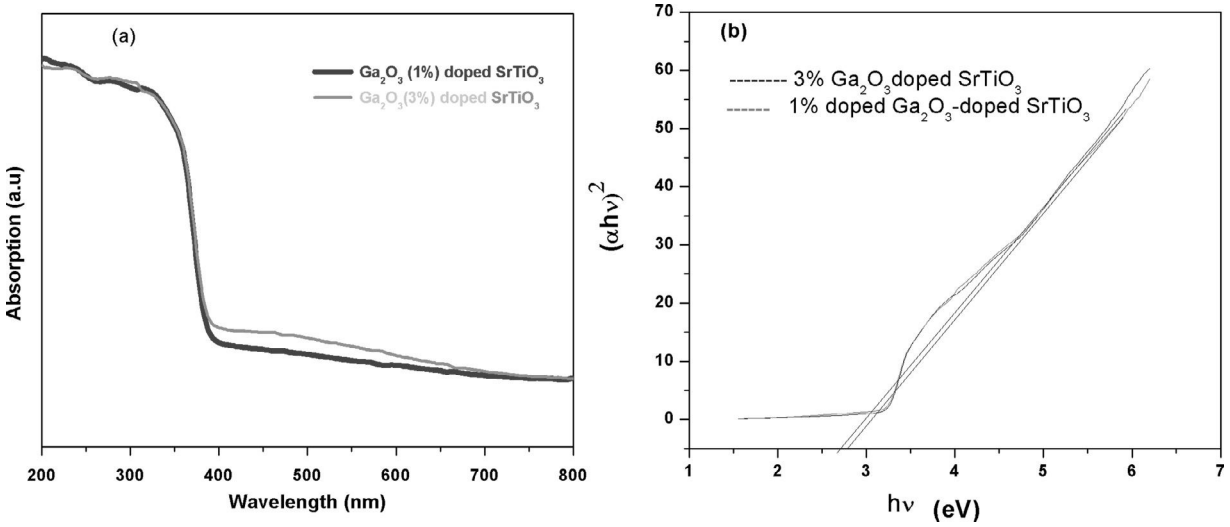

Fig. 5. (a) UV-absorption spectra and (b) Tauc plot of 1% and 3% Ga_2O_3-doped $SrTiO_3$ samples.

ture of $SrTiO_3$ via the Tauc plots. The energy gap values were determined around 3.11 eV and 3.07 eV for 1% and 3% Ga_2O_3 doped STO samples from the Tauc plot using optical absorption data. The energy gap decreasing of $SrTiO_3$ material with the increasing of Mn impurity concentration was reported by Wu et al. [7], which are correlate the phenomena with obtained energy gap values of Ga_2O_3 doped $SrTiO_3$ samples. This was due to the red shift was happened in the optical absorption spectra. In addition, optical band gap values are decreased with the addition of Ga_2O_3 doped into the host lattice $SrTiO_3$. This decreasing optical band gap could have occurred, when the light source interacts with the Ga_2O_3 dopant incorporated into the host lattice to create a multi-inner energy state in the valence band and conduction band.

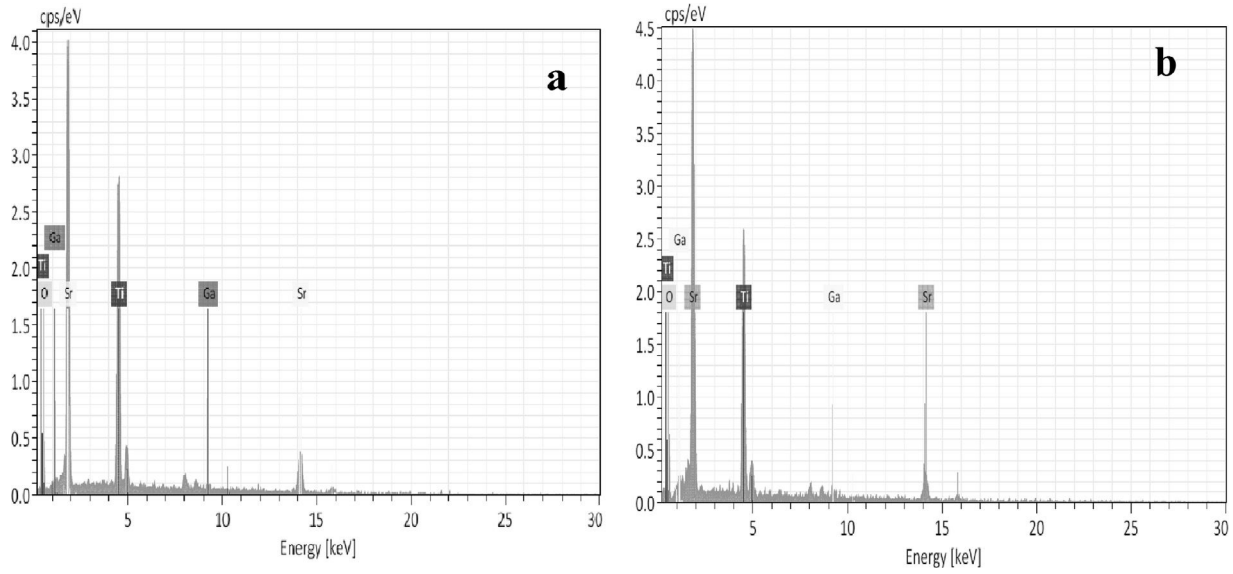

Fig. 6. EDX spectra of (a) 1% and (b) Ga_2O_3 (3%) doped $SrTiO_3$ samples.

3.7. Energy dispersive X-ray (EDX) spectra analysis

We traced only strontium (Sr), titanium (Ti) and oxygen (O) with gallium (Ga) elements in the EDX images of the Ga_2O_3 doped $SrTiO_3$ prepared samples as displayed in Fig. 6. These results indicate the evidence of the incorporation of Ga in strontium material. For the 1% Ga doped sample, the Sr element peak was located at energy level of 1.98 and 14 keV. In addition, the Ti element's position peak is at energy (0.5 and 4.5 KeV). Moreover, the O element is located at energy 0.51 KeV. The Ga element is position peak at 0.48 and 6.2 KeV, respectively. For the 3% Ga doped sample, we noticed the Sr peak position at energy (1.98 and 14.1KeV), Ti peak at energy (0.2 and 4.5 KeV), O element peaks at energy (0.5 KeV) and Ga element at 1.1 and 9.2KeV), respectively. Based on the EDX results, the peak position energy level is slightly changed due to the galium oxide dopant concentration in the host lattice.

3.8. X-ray photoelectron spectroscopy (XPS) analysis

The chemical oxidation state of metals and non-metal elements and their corresponding binding energy of the 3% Ga_2O_3 doped $SrTiO_3$ sample are presented in XPS, as represented in Fig. 7. In the Ga_2O_3 doped $SrTiO_3$ sample (Fig. 7a), metals like Sr, Ti, Ga and the non-metal (O) element were traced in the XPS. The deconvolution spectra of the Sr 3d ion are illustrated in Fig. 7b. A strong spin-orbit interaction between the Sr ($3d_{3/2}$) and Sr ($3d_{1/2}$) has been found. The binding energies of Sr ($3d_{3/2}$) and Sr ($3d_{1/2}$) positions are 133 and 134.6 eV [1]. When the Ga impurity is introduced into the $SrTiO_3$ material, the drift in the binding energy of Sr 3d state is forwarded to the lower edge in the XPS studies. In addition, it showed that Ti^{3+} signals were detected (Fig. 7c), giving Ti^{3+}/Ti^{4+} proportion of the 7.0 eV for Ga doped $SrTiO_3$ sample. The binding energies of Ti ($2P_{3/2}$) and Ti ($2P_{1/2}$) states are located at 458.1 and 463.8 eV [1]. In addition, the strong spin -orbit effect is displayed for the Ti (2p) state and is evident of the symmetric interaction between the Ti ($2p_{3/2}$) and Ti ($2p_{1/2}$) states and also between the Sr ($3d_{3/2}$) and Sr ($3d_{1/2}$) states. The position of the chemical oxidation state of the non-metal (oxygen) in the 3% Ga doped $SrTiO_3$ sample is shown in Fig. 7d. Fig. 7d, records the binding energy around 528.2 and 530.2 eV. In the Ga3d5 spectrum the peak was observed in 19.2 eV and it has been attributed to the trivalent Ga ion. Finally, based on the above XPS studies, it is confirmed that the Ga dopant has been incorporated into the $SrTiO_3$ lattice. Furthermore, the XPS spectra have shown that the oxygen vacancy is present in the gallium oxide doped $SrTiO_3$ material.

3.9. Dielectric analysis

Fig. 8 (a&b) displays the frequency dependent dielectric constant of the Ga_2O_3 doped $SrTiO_3$ samples at different temperatures (305, 323, 373, 423, 437, 523 and 573 K). In general, the polarization will be highly responsive in the lower frequency portion and inactive in the higher frequency region in nanomaterials samples [38]. In Fig. 8, we could notice that the high dielectric constants were observed in the lower frequency portion; this was because of the presence of interfacial polarization [39].

The electrons present in the samples were not able to remain within the field, when the frequency of the applied electric field increased and as a result, their directional delays beyond the field applied were altered. This was due to the interfacial polarization disappeared in the high frequency portion, which reduced the relative permittivity (dielectric constant). We could see that the 3% Ga_2O_3 doped $SrTiO_3$ observed high relative permittivity (40000) at lower frequency portion compared to that of the 1% Ga_2O_3 doped sample (dielectric constant value ~ 10000) at 573K. In addition, the dielectric constant values of both the Ga_2O_3 doped $SrTiO_3$ samples increased with increasing temperatures [31]. This was due to the increasing contribution of space charge polarization [31].

Fig. 9 (a&b) displayed the frequency dependent dielectric loss of the Ga_2O_3 doped $SrTiO_3$ samples at various temperatures. When there is an increase in the applied frequency, the dielectric loss gently decreases as exhibited in Fig. 9. We could detect that in the 3% Ga_2O_3 doped $SrTiO_3$ sample, the dielectric loss value is slightly lesser compared to that of the 1% Ga_2O_3 doped sample. The lower dielectric constant values obtained for the 3% doped $SrTiO_3$ sample suggested its excellent dielectric properties.

In addition, the variation of the dielectric constant values of Ga_2O_3 doped samples depends on the temperatures. From the Fig. 9, we could notice that the dielectric loss increases with increasing of temperatures for the 1% and 3% Ga_2O_3 doped $SrTiO_3$ samples. This was due to the thermally activated behavior of the dielectric relaxation of the system [40].

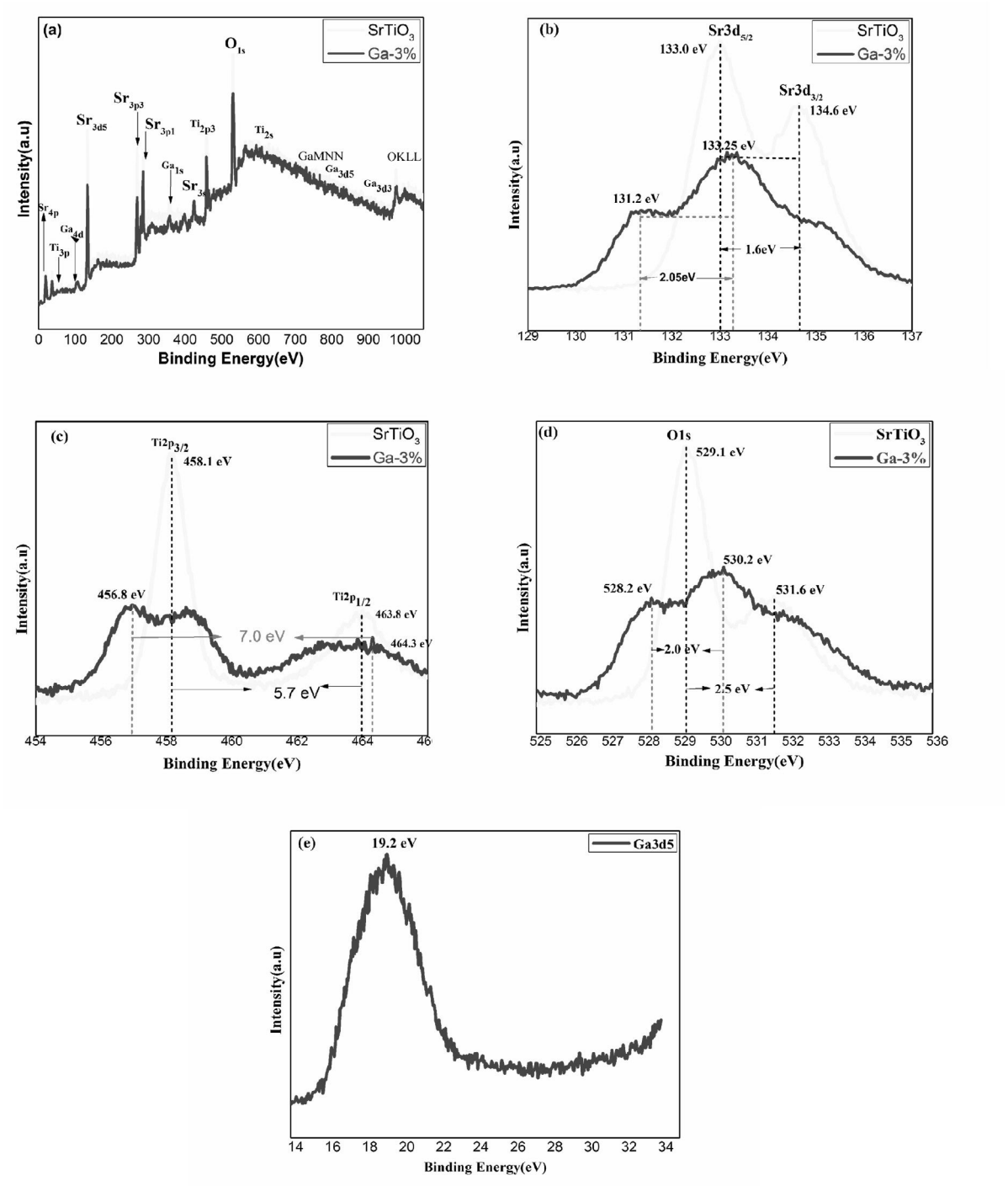

Fig. 7. XPS of 3% Ga_2O_3 doped $SrTiO_3$ sample.

3.10. Electrical conductivity analysis

Fig. 10 (a&b) demonstrates the frequency dependent electrical conductivity of the 1% and 3% Ga_2O_3 doped $SrTiO_3$ samples at various temperatures. From Fig. 10, the 3% Ga_2O_3 doped $SrTiO_3$ sample was observed to have slightly higher electrical conductivity compared to the 1% of Ga_2O_3 doped sample. Generally, electrical conductivity increases as the optical band of nanomaterials is reduced. Based on the above concept, a slightly higher electrical conductivity was observed for the 3% Ga_2O_3 doped $SrTiO_3$, which is in good agreement with the obtained optical band gap (E_g) value of the 3% Ga_2O_3 doped (3.07 eV) compared to that of the 1% Ga_2O_3 doped $SrTiO_3$ material (($E_g = 3.11$ eV). In addition, From the Fig. 10, we could observed that the electrical conductivity increases with an increasing the temperatures. This was due to the movement of hopping of charge carriers between the ions present in the material [40,41]. The behavior of conductivity exhibits two distinct portions in the studied frequency range. In the low frequency region, the charge carriers have ample time to assemble at the interfaces of the electrode, and hence result in the electrode polarization ef-

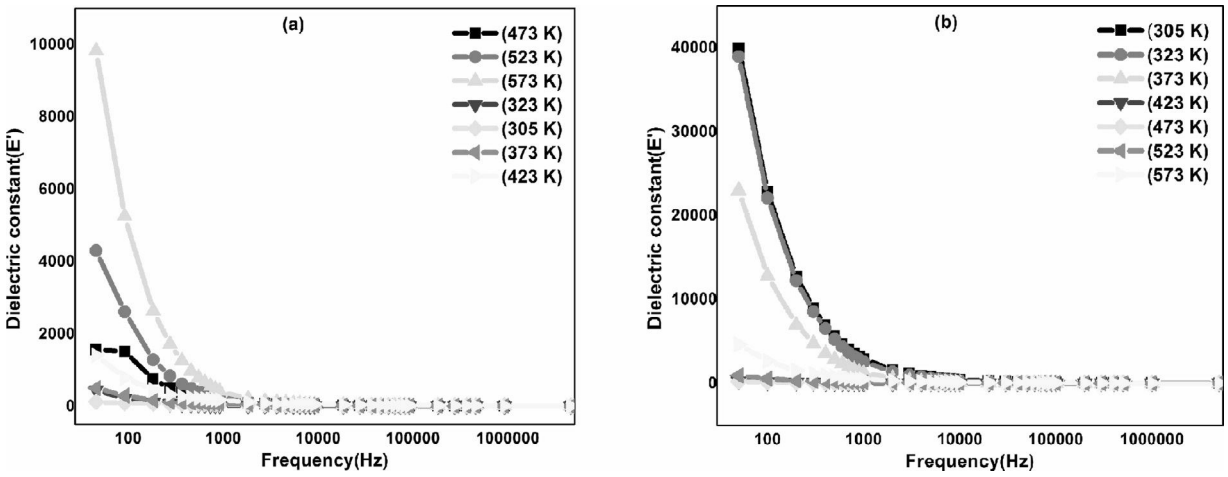

Fig. 8. Frequency dependent dielectric constant of (a) 1% and (b) 3% Ga_2O_3-doped $SrTiO_3$ samples.

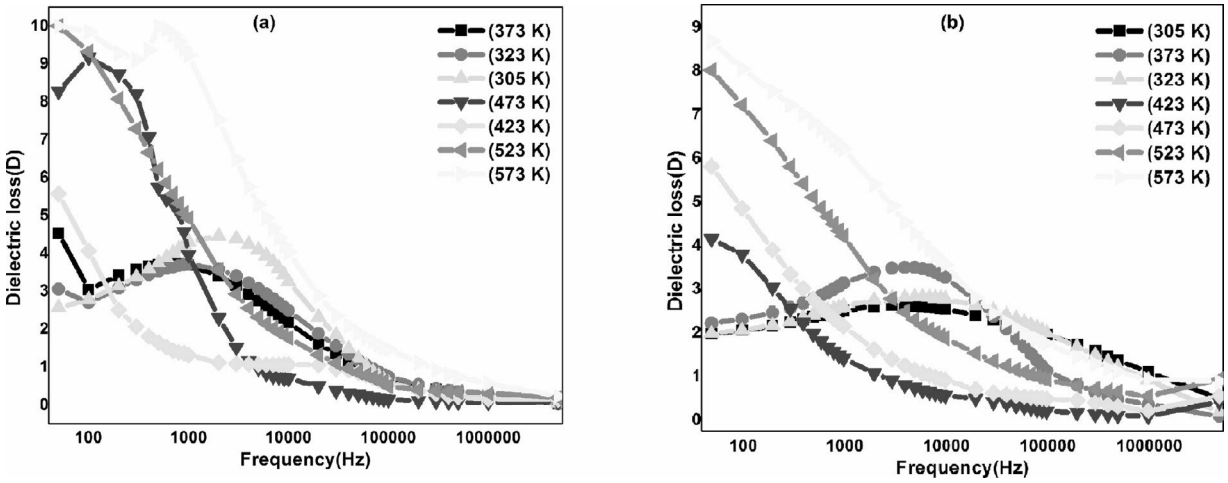

Fig. 9. Frequency dependent dielectric loss of (a) 1% and (b) 3% Ga_2O_3- doped $SrTiO_3$ samples.

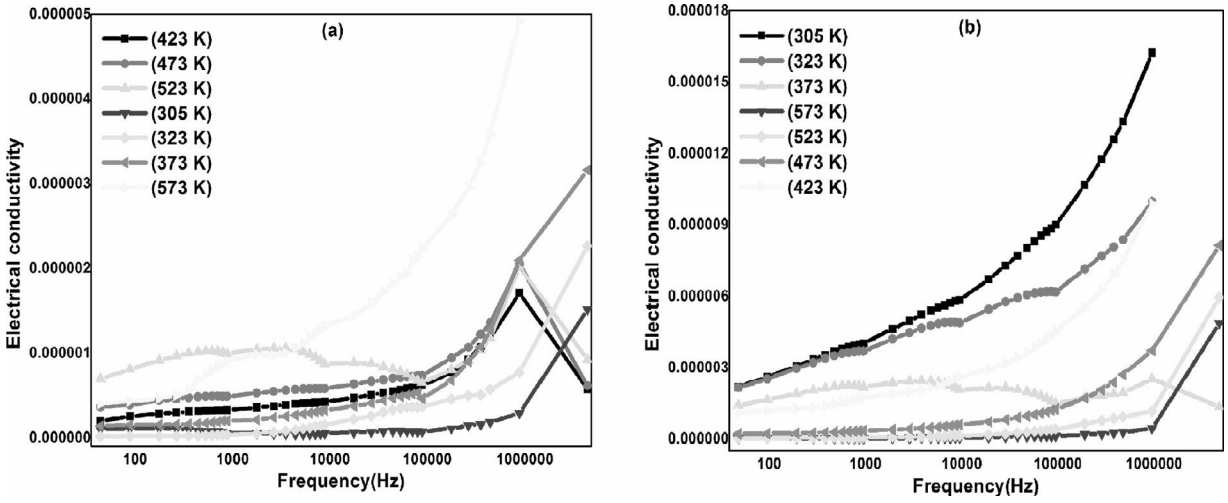

Fig. 10. Electrical conductivity of (a) 1% and (b) 3% Ga_2O_3 doped $SrTiO_3$ samples.

fect [42]. The conductivity is less at the low frequency scale due to the presence of the grain boundary effect, which corresponds to the absence of the mobility charge carriers [43]. Moreover, the change in the electrical conductivity values of the Ga_2O_3 doped samples in the higher frequency region depends on the temperatures.

4. Conclusions

In summary, we synthesized 1% and 3 wt% of Ga_2O_3 doped $SrTiO_3$ material via the mechanochemical synthesis followed by the calcination process. The XRD pattern of the synthesized Ga_2O_3 doped $SrTiO_3$ materials confirmed the presence of a single phase

and cubic perovskite crystal structure. The Sr-O and Ti-O bond and feasible incorporation of gallium oxide ions into the parent lattice were detected by the FT-IR analysis. The Raman modes showed that the cubic phase of $SrTiO_3$ was confirmed which was supported by the cubic structure obtained from the XRD data. Non-uniform spherical and irregular sheets/spherical particles were identified from the morphology studies. The 3% Ga_2O_3 doped $SrTiO_3$ material has a slightly reduced energy gap relative to the 1% Ga_2O_3 doped sample, and this was confirmed by optical spectra studies. The possible oxidation states of elements, the main drift in the binding energy of the elements, and surface defects (oxygen vacancy) in the synthesized Ga_2O_3-doped $SrTiO_3$ material have been discussed in the XPS studies. The frequency dependent range's relative permittivity and dielectric losses have been examined while the space charge polarization occurs. Hence the Ga_2O_3-doped $SrTiO_3$ ceramic compounds can find potential applications in the fabrication of optoelectronic devices.

Declaration of Competing Interest

The authors declare that they have no known competing financial interest or personel relationship that could have appeared to influence the work reported in this paper.

CRediT authorship contribution statement

G. Saravanan: Methodology, Writing - original draft. **K. Ramachandran:** Investigation, Writing - original draft, Writing - review & editing. **J. Gajendiran:** Investigation, Writing - original draft, Writing - review & editing. **S. Gnanam:** Writing - review & editing.

Acknowledgements

The authors convey their heart full of gratitude to the Nano Technology Research Centre in SRM University. The authors also would like to express their sincere thanks to IIT Madras, Pondicherry University for granting permission to take XPS studies, Raman spectrum and dielectric studies related to instrumentation. No funds are received from any other funding agencies.

References

[1] A. Karaphun, S. Hunpratub, E. Swatsitang, Effect of annealing on magnetic properties of Fe-doped $SrTiO_3$ nanopowders prepared by hydrothermal method, Microelectron. Eng. 126 (2014) 42–48.
[2] R. Li, F. Liu, C. Zhang, J. Liu, J. Zhou, L. Xu, Electrical properties of Fe–doped $SrTiO_3$ with B-site-deficient for SOFC anodes, Ceram. Int. 45 (2019) 21684–21687.
[3] X. Wang, Z. Wang, Q. Hu, C. Zhang, D. Wang, L. Li, Room temperature multiferroic properties of Fe-doped nonstoichiometric $SrTiO_3$ ceramics at both A and B sites, Solid State Commun. 289 (2019) 22–26.
[4] H. Fujishita, Y. Arai, H. Okamoto, T. Yamaguchi, Low temperature dielectric and magnetic properties of Fe-ion-doped $SrTiO_3$, Phys. B 521 (2017) 1–5.
[5] A. Lacz, L. Lancucki, R. Lach, B. Kamecki, E. Drozdz, Structural and electrical properties of Cr-doped $SrTiO_3$ porous materials, Int. J. Hydrogen Energy 43 (2018) 8999–9005.
[6] D. Yang, X. Zhao, X. Zou, Z. Zhou, Z. Jiang, Removing Cr (VI) in water via visible-light photocatalytic reduction over Cr-doped $SrTiO_3$ nanoplates, Chemosphere 215 (2019) 586–595.
[7] G. Wu, P. Li, D. Xu, B. Luo, Y. Hong, W. Shi, C. Liu, Hydrothermal synthesis and visible-light-driven photocatalytic degradation for tetracycline of Mn–doped $SrTiO_3$ nanocubes, Appl. Surf. Sci. 333 (2015) 39–47.
[8] V. Trepakov, M. Makarova, O. Stupakov, E.A. Tereshina, J. Drahokoupil, M. Cernanský, et al., Synthesis, structure and properties of heavily Mn-doped perovskite-type $SrTiO_3$ nanoparticles, Mater. Chem. Phys. 143 (2014) 570–577.
[9] Y. Qiao, W. Li, Y. Zhang, L. Jing, C. Gao, W. Cao, et al., Hole-pinned defect-dipoles induced colossal permittivity in Bi doped $SrTiO_3$ ceramics with Sr deficiency, J. Mater. Sci. Technol. 44 (2020) 54–61.
[10] M.H. Fisoldin, M.S. Idris, R.A.M. Osman, K.N.D.K. Muhsen, Z.A.Z. Jamal1, Electrical properties of Sn doped $SrTiO_3$, AIP Conf. Proceed. 2203 (2020) 020044.
[11] I.A. Sluchinskaya, A.I. Lebedev, electronic and magnetic properties of structural defects in $SrTiO_3$ (Co), J. Alloys Comp. 820 (2020) 153243.
[12] J. Xu, Y. Wei, Y. Huang, J. Wang, X. Zheng, Z. Sun, et al., Solvothermal synthesis nitrogen doped $SrTiO_3$ with high visible light photocatalytic activity, Ceram. Int. 40 (2014) 10583–11059.
[13] I. Tamiolakis, D. Liu, F.X. Xiao, J. Xie, I.T. Papadasd, T. Salim, et al., Mesoporous implantable Pt/$SrTiO_3$:C,N nanocuboids delivering enhanced photocatalytic H_2-production activity via plasmon-induced interfacial electron transfer, Appl. Catal. B: Environ. 236 (2018) 338–347.
[14] M. Qin, F. Gao, J. Cizek, S. Yang, X. Fan, L. Zhao, et al., Point defect structure of La-doped SrTiO3 ceramics with colossal Permittivity, Acta Mater. 164 (2019) 76–89.
[15] J. Liu, C.L. Wang, Y. Li, W.B. Su, Y.H. Zhu, J.C. Li, L.M. Me, Influence of rare earth doping on thermoelectric properties of $SrTiO_3$ ceramics, J. Appl. Phys. 114 (2013) 223714.
[16] P. Blennow, A. Hagen, K.K. Hansen, L. Reine Wallenberg, M. Mogensen, Defect and electrical transport properties of Nb-doped $SrTiO_3$, Solid State Ion. 179 (2008) 2047–2058.
[17] I. Velasco-Davalos, F. Ambriz-Vargas, R. Thomas, Ruediger, surface preparation of (110) oriented pure and Nb doped $SrTiO_3$ single crystal substrates by microwave assisted hydrothermal method, Surf. Coat. Technol. 283 (2015) 108–114.
[18] J.Q. Zheng, Y.J. Zhu, J.S. Xu, B.Q. Lu, C. Qi, F. Chen, J. Wu, Microwave assisted rapid synthesis and photocatalytic activity of mesoporous Nd-doped $SrTiO_3$ nanospheres and nanoplates, Mater. Lett. 100 (2013) 62–65.
[19] A.M. Dehkordi, S. Bhattacharya, J. He, H.N. Alshareef, T.M. Tritt, Significant enhancement in thermoelectric properties of polycrystalline Pr-doped $SrTiO_3$ -δ ceramics originating from nonuniform distribution of Pr dopants, Appl. Phys. Lett. 104 (2014) 193902.
[20] X. Wang, Q. Hu, L. Li, X. Lu, Effect of Pr substitution on structural and dielectric properties of $SrTiO_3$, J. Appl. Phys. 112 (2012) 044106.
[21] A.M. Dehkordi, S. Bhattacharya, T. Darroudi, J.W. Graff, U. Schwingenschlögl, H.N. Alshareef, et al., Large thermoelectric power factor in Pr-doped $SrTiO_3$-δ ceramics via grain-boundary-induced mobility enhancement, Chem. Mater. 26 (2014) 2478–2485.
[22] D.K. Singh, J. Manam, D.K. Singh, J. Manam, Optical spectroscopic and thermal quenching behaviour of perovskite $SrTiO_3$:Sm^{3+} orange emitting phosphors for lighting applications, J. Mater. Sci.: Mater. Electron. 29 (2018) 5579–5588.
[23] G. Saravanan, K. Ramachandran, J. Gajendiran, E. Padmini, Effect of ceria concentration of Strontium titanate on the structural, optical, dielectric and electrical properties, Chem. Phys. Lett. (2020) 137314.
[24] M. Abdi, V. Mahdikhah, S. Sheibani, Visible light photocatalytic performance of La-Fe co- doped $SrTiO_3$ perovskite powder, Opt. Mater. 102 (2020) 109803.
[25] D. Luo, W. Xiao, F. Lin, C. Luo, X. Li, Effects of a-site deficiency on the electrical conductivity and stability of (La, Co) co-doped $SrTiO_3$ anode materials for intermediate temperature solid oxide fuel cells, Adv. Powder Technol. 27 (2016) 481–485.
[26] J. Han, Q. Sun, Y. Song, J. Han, Q. Sun, Y. Song, Enhanced thermoelectric properties of La and Dy co-doped, Sr-deficient $SrTiO_3$ ceramics, J. Alloys Comp. 705 (2017) 22–27.
[27] C.Y. Guo, X. Qi, RF magnetron sputter deposition and electrical properties of La and Y doped $SrTiO_3$ epitaxial films, Mater. Des. 179 (2019) 107888.
[28] T.S. Jamil, H.A. Abbas, A.M. Youssief, E.S. Mansor, F.F. Hammad, The synthesis of nano-sized undoped, Bi doped and Bi, Cu co-doped $SrTiO_3$ using two sol-gel methods to enhance the photocatalytic performance for the degradation of dibutyl phthalate under visible light, C, R. Chimie. 20 (2017) 97–106.
[29] J. Liu, Q. Liu, Z. Nie, S. Nie, D. Lu, P. Zhu, Dielectric relaxations in fine-grained $SrTiO_3$ ceramics with Cu and Nb co doping, Ceram. Int. 45 (2019) 10334–10341.
[30] J.H. Lin, C.S. Hwang, F.R. Sie, Preparation and thermoelectric properties of Nd and Dy co- doped $SrTiO_3$ bulk materials, Mater. Res. Bull. 122 (2020) 110650.
[31] M.S. Alkathy1, K.C. James Raju1, Effect of Bi and Li co-substituted $SrTiO_3$ ceramics on structural and dielectric properties, J. Mater. Sci.: Mater. Electron. 27 (2016) 8957–8965.
[32] J. Chen, T. Sekiguchi, J. Li, S. Ito, W. Yi, A. Ogura, Investigation of dislocations in Nb-doped $SrTiO_3$ by electron-beam-induced current and transmission electron microscopy, Appl. Phys. Lett. 106 (2015) 102109.
[33] B.V. Prasad, G. Narsinga Rao, J.W. Chen, D. Suresh Babu, Abnormal high dielectric constant in $SmFeO_3$ semiconductor ceramics, Mater. Res. Bull. 46 (2011) 1670–1673.
[34] V. Eswaramoorthi, S. Sebastian, R. Victor Williams, Influence of Ga doping on the structural optical and electrical properties of $Ba_{0.6}Sr_{0.4}TiO_3$ Thin films, Int. J. Sci. Technol. 4 (2015) 86–91.
[35] S.D. Shenoy, P.A. Joy, M.R. Anantharaman, Effect of mechanical milling on the structural, magnetic and dielectric properties of Co precipitated ultrafine zinc ferrite, J. Magn. Magn. Mater. 269 (2004) 217–226.
[36] X. Wei, G. Xu, Z.H. Ren, Y.G. Wang, G. Shen, G.R. Han, Composition and shape control of single-crystalline $Ba_{1-x}Sr_xTiO_3$ (x = 0-1) nano crystals via a solvothermal route, J. Cryst. Growth 310 (2008) 4132–4137.
[37] F.A. Rabuffetti, H.S. Kim, J.A. Enterkin, Y.M. Wang, C.H. Lanier, L.D. Marks, et al., Synthesis-dependent first-order raman scattering in $SrTiO_3$ nanocubes at room temperature, Chem. Mater. 20 (2008) 5628–5635.

[38] T. Xian, H. Yang, L. Di, J. Ma, H. Zhang, J. Dai, Photocatalytic reduction synthesis of $SrTiO_3$-graphene nanocomposites and their enhanced photocatalytic activity, Nanoscale Res. Lett. 9 (2014) 327.
[39] M.C.F. Alves, S.C. Souza, H.H.S. Lima, M.R. Nascimento, M.R.S. Silva, J.W.M. Espinosa, et al., Influence of the modifier on the short and long range disorder of stannate perovskites, J. Alloys Comp. 476 (2009) 507–512.
[40] S. Sagadevan, S. Vennila, J. Anita Lett, A.R. Marlinda, N.A.B. Hamizi, M.R. Johan, Tailoring the structural, morphological, optical, thermal and dielectric characteristics of ZnO nanoparticles using starch as a capping agent, Results Phys. 15 (2019) 102543.
[41] U. Adem, N. Mufti, A.A. Nugroho, G. Catalan, B. Noheda, T.T.M. Palstra, Dielectric relaxation in $YMnO_3$ single crystals, J. Alloys Comp. 638 (2015) 228–232.
[42] Y. Xu, T. Liu, Y. He, X. Yuan, Dielectric properties of Ba0.6Sr0.4TiO3-Sr(Ga0.5Ta0.5)O3 solid solutions, IEEE Trans. Ultrason. Ferroelectr. Freq. Cont. 55 (2008) 2369-2376.
[43] R. Schmidt, A. Basu, A.W. Brinkman, Z. Klusek, P.K. Datta, Electron-hopping modes in $NiMn_{(2)}O_{(4+\delta)}$ materials, Appl. Phys. Lett. 86 (2005) 501–503.